NEUROSCIENCE

Recovery of walking after paralysis by regenerating characterized neurons to their natural target region

Jordan W. Squair[1,2,3]*†, Marco Milano[1,3]†, Alexandra de Coucy[1,3], Matthieu Gautier[1,3], Michael A. Skinnider[1,3], Nicholas D. James[1,3], Newton Cho[1,3], Anna Lasne[1,3], Claudia Kathe[1,3], Thomas H. Hutson[1,3,4], Steven Ceto[1,3], Laetitia Baud[1,3], Katia Galan[1,3], Viviana Aureli[1,2,3,5], Achilleas Laskaratos[3,5], Quentin Barraud[1,3], Timothy J. Deming[6], Richie E. Kohman[4], Bernard L. Schneider[1,7,8], Zhigang He[9], Jocelyne Bloch[1,2,3,5], Michael V. Sofroniew[10]‡, Gregoire Courtine[1,2,3,5]*‡, Mark A. Anderson[1,3,4,5]*‡

Axon regeneration can be induced across anatomically complete spinal cord injury (SCI), but robust functional restoration has been elusive. Whether restoring neurological functions requires directed regeneration of axons from specific neuronal subpopulations to their natural target regions remains unclear. To address this question, we applied projection-specific and comparative single-nucleus RNA sequencing to identify neuronal subpopulations that restore walking after incomplete SCI. We show that chemoattracting and guiding the transected axons of these neurons to their natural target region led to substantial recovery of walking after complete SCI in mice, whereas regeneration of axons simply across the lesion had no effect. Thus, reestablishing the natural projections of characterized neurons forms an essential part of axon regeneration strategies aimed at restoring lost neurological functions.

The transected axons of injured central nervous system neurons can now be induced to regenerate through and across anatomically complete spinal cord injury (SCI) with multipronged treatments that reactivate latent growth programs and provide chemoattractive growth factors (*1*–*4*). Analogously, immature neural progenitors grafted into complete SCI lesions can attract host axons into lesions and can extend their axons out of lesions to grow extensively throughout the central nervous system (*5*, *6*). However, despite the extensive axon regeneration achieved by these and related approaches (*7*, *8*), reproducible restoration of functions has been elusive, suggesting that essential yet unidentified mechanisms to restore neurological functions have yet to be identified.

Whether robust restoration of function will require targeting specific neurons and regenerating the axons of these neurons not simply across lesions but also guiding them to reach their natural target region is unknown. To address this question, we studied neuronal subpopulations in the spinal cord that can restore walking by relaying supraspinal commands past severe but incomplete SCI (*9*–*11*). We hypothesized that regenerating the transected axons of neuronal subpopulations that are essential for recovery after incomplete SCI to reach simply across anatomically complete lesions will fail to improve functional recovery, whereas chemoattracting and guiding the axons of these neurons to reach their distal natural target region in the lumbar spinal cord would mediate substantial recovery of walking.

Characterizing neurons involved in natural recovery

The lumbar spinal cord hosts the neuronal subpopulations that produce walking. Unilateral hemisections (Brown-Séquard syndrome) deprive these neurons of essential supraspinal inputs to produce walking on the injured side. Yet, both humans and animal models recover bilateral walking after these injuries (*12*, *13*). Our and other previous studies showed that, in this scenario, neurons located in the midthoracic spinal cord relay supraspinal commands past the lateral hemisection to restore walking (*9*–*11*). Even after temporally and spatially separated, opposite-side hemisection lesions that interrupt all direct projections from the brain to the lumbar spinal cord, these neurons can still relay sufficient supraspinal input to restore bilateral walking (*9*–*11*). Ablation of these neurons in the thoracic spinal cord did not alter walking in the absence of injury but eliminated the natural recovery of walking observed after unilateral or bilateral hemisections (*9*, *14*). Therefore, we aimed to dissect the molecular and anatomical properties of the neuronal subpopulations underlying this natural recovery.

To identify the neuronal subpopulat… with projections to the lumbar spinal cord, … injected recombinant adeno-associated virus 2 (rAAV2) encoding enhanced green fluorescent protein (eGFP) fused to the nuclear envelope protein KASH into the lumbar spinal cord of uninjured mice (fig. S1A). This strategy labeled the nuclei of neurons with direct projections to the lumbar spinal cord throughout the central nervous system, including putative relay neurons in the midthoracic spinal cord (fig. S1A), and enabled fluorescence-activated nuclei sorting coupled to single-nucleus RNA sequencing (snRNA-seq) of projection-specific neuronal subpopulations (Fig. 1A and fig. S1, B and C).

We profiled the midthoracic spinal cord with snRNA-seq and obtained high-quality transcriptional profiles from 122 $eGFP^{ON}$ and 2823 $eGFP^{OFF}$ nuclei (fig. S1, D to I). Unsupervised clustering identified all of the major cell types of the spinal cord (fig. S1, J to M). We then subjected the neurons to a second round of clustering, which identified 28 subpopulations that expressed canonical marker genes (Fig. 1B and fig. S2A). Our taxonomy parcellated neurons into cardinal classes, including motor-sensory, local-long range, and excitatory-inhibitory subpopulations (fig. S2, B to D) (*15*). The 105 $eGFP^{ON}$ neurons were primarily found within a single ventral neuronal subpopulation of thoracic neurons (Hoxa7) that expressed the marker Vsx2 plus a marker of long-distance projection neurons, Zfhx3 Z-group neurons (*15*), which we named spinal cord $(SC)^{Vsx2::Hoxa7:Zfhx3\rightarrow lumbar}$ neurons (Fig. 1C and fig. S2, E and F).

Because these neurons express Vsx2 (*16*, *17*), they derive from developmentally defined V2a neurons. Vsx2-expressing neurons are found in different locations along the neuraxis, including the brainstem (*18*), cervical spinal cord (*19*–*21*), and lumbar spinal cord (*22*–*25*), where they exhibit a variety of projection patterns (*26*–*30*). Accordingly, the distinct properties of different subpopulations of Vsx2-expressing neurons dictate and restrict their specific contribution to neurological functions, such as reaching (*19*, *21*, *31*) and walking (*18*, *22*, *23*, *25*, *31*–*34*). Indeed, although developmentally defined V2a neurons located in the lumbar spinal cord have been implicated in the production of walking (*18*, *22*, *23*, *31*–*34*), the ablation of all neurons in the thoracic spinal cord, including those expressing Vsx2, has no detectable impact on walking in uninjured rodents (*9*, *14*).

Given that thoracic neurons only become essential to walking after incomplete SCI (*9*), we asked whether $SC^{Vsx2::Hoxa7:Zfhx3\rightarrow lumbar}$ neurons are transcriptionally perturbed after natural recovery. We compared neuronal nuclei from uninjured mice and mice that had recovered walking (Fig. 1, D and E, and fig. S3, A to E) after temporally and spatially separated lateral hemisection SCIs (fig. S4A and movie S1). High-quality transcriptional profiles were obtained

[1]NeuroX Institute, School of Life Sciences, Swiss Federal Institute of Technology (EPFL), 1015 Lausanne, Switzerland. [2]Department of Neurosurgery, Lausanne University Hospital (CHUV) and University of Lausanne (UNIL), 1005 Lausanne, Switzerland. [3]Defitech Center for Interventional Neurotherapies (NeuroRestore), CHUV/UNIL/EPFL, 1005 Lausanne, Switzerland. [4]Wyss Center for Bio and Neuroengineering, 1202 Geneva, Switzerland. [5]Department of Clinical Neuroscience, Lausanne University Hospital (CHUV) and University of Lausanne (UNIL), 1005 Lausanne, Switzerland. [6]Departments of Bioengineering, Chemistry and Biochemistry, University of California, Los Angeles, Los Angeles, CA 90095, USA. [7]Bertarelli Platform for Gene Therapy, Swiss Federal Institute of Technology (EPFL), 1015 Lausanne, Switzerland. [8]Brain Mind Institute, School of Life Sciences, Swiss Federal Institute of Technology (EPFL), 1015 Lausanne, Switzerland. [9]F.M. Kirby Neurobiology Center, Department of Neurology, Boston Children's Hospital, Harvard Medical School, Boston, MA 02115, USA. [10]Department of Neurobiology, David Geffen School of Medicine, University of California, Los Angeles, Los Angeles, CA 90095, USA.
***Corresponding author. Email: gregoire.courtine@epfl.ch (G.C.); mark.anderson@epfl.ch (M.A.A.); jordan.squair@epfl.ch (J.W.S.)**
†These authors contributed equally to this work.
‡These authors contributed equally to this work.

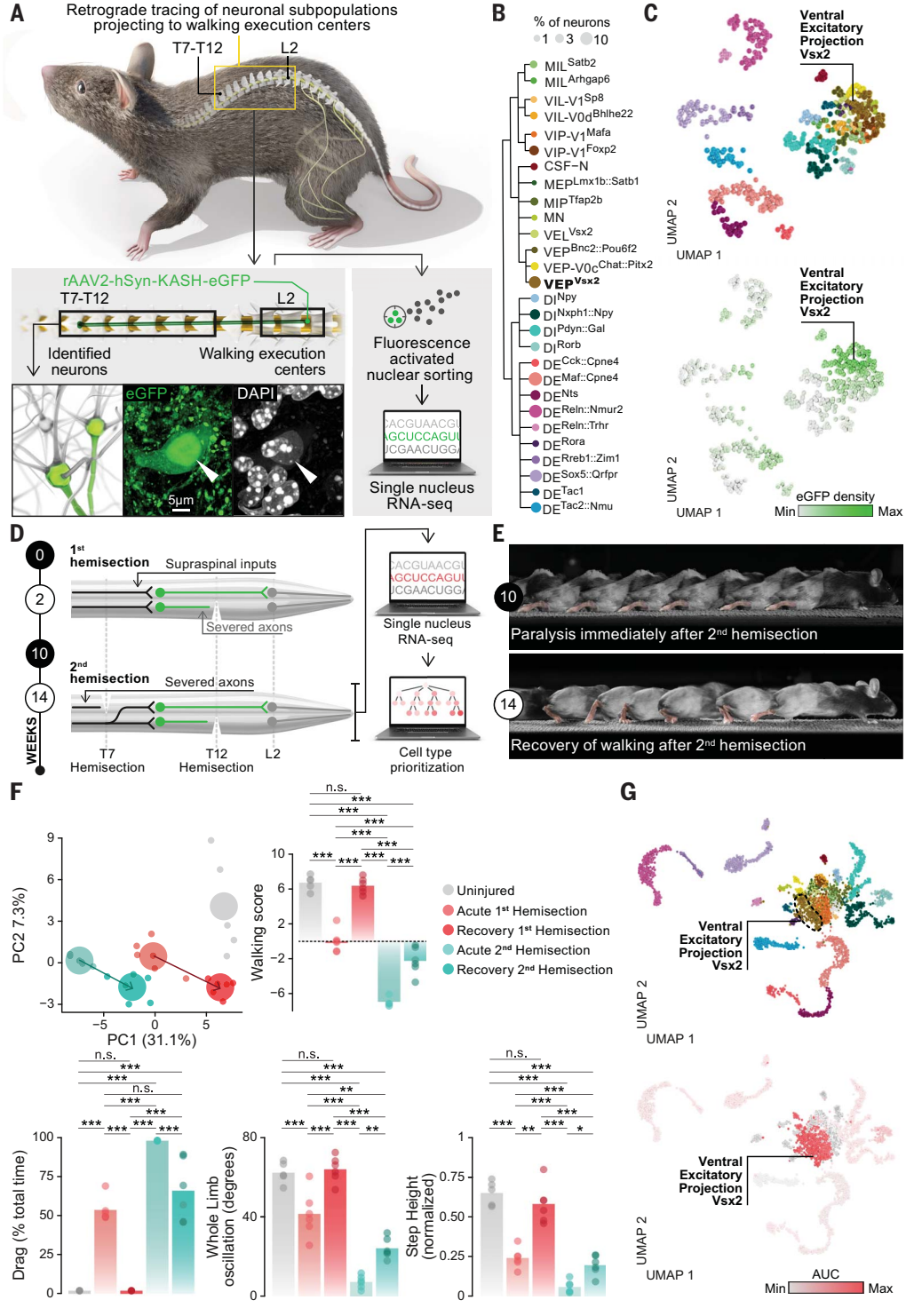

Fig. 1. Transcriptional identification of neurons underlying natural spinal cord repair. (**A**) Overview of the experimental approach enabling projection-specific single-nucleus RNA sequencing (snRNA-seq) of neuronal subpopulations projecting from the thoracic spinal cord to walking execution centers. (**B**) Clustering tree of neuronal subpopulations in the thoracic spinal cord. (**C**) Uniform manifold approximation and projection (UMAP) visualization of neuronal nuclei revealing 28 neuron subpopulations (left). Individual nuclei are colored by the proportion of their nearest neighbors obtained from sorted projection neurons (eGFP density), revealing a primary origin from $SC^{Vsx2::Hoxa7::Zfhx3\rightarrow lumbar}$ neurons (right). (**D**) Overview of the experimental approach enabling snRNA-seq after natural spinal cord repair. (**E**) Chronophotography of mice before and after natural spinal cord repair. (**F**) Walking was quantified using principal component analysis applied to gait parameters calculated from kinematic recordings. In this denoised space, each dot represents a mouse (n > 10 gait cycles per mouse, n = 6 mice per group, n = 5 mice in the uninjured group). Larger dots represent the mean of each experimental group. The first principal component (PC1) distinguished gaits from mice without SCI from mice with the most severe paralysis, found immediately after the second hemisection. Walking scores were thus quantified as the scores on PC1. Analysis of factor loadings on PC1 revealed that the percentage of paw dragging, the extent of whole-limb oscillation (virtual limb connecting the hip to the toe), and step height were the parameters that showed high correlation with PC1. Bars report the mean values of these gait parameters. Raw data and statistics and provided in data S2. (**G**) UMAP visualization of neuronal nuclei revealing 28 neuron subpopulations (top) and colored by Augur cell type prioritization (AUC, area under the curve), identifying perturbation-responsive neuronal subpopulations when comparing mice that had undergone natural repair versus uninjured mice (bottom).

from 9264 nuclei (fig. S4, B to K) and were integrated with our projection-specific snRNA-seq experiment, wherein we identified and evaluated the same 28 neuronal subpopulations (Fig. 1G and fig. S4, L to O). Cell type prioritization (*35*, *36*) revealed that $SC^{Vsx2::Hoxa7::Zfhx3\rightarrow lumbar}$ neurons exhibited the most pronounced transcriptional response across all neuronal subpopulations embedded in the thoracic segments of mice that had recovered walking (Fig. 1G and fig. S4, N to Q), and Gene Ontology analysis (fig. S4R) revealed that these transcriptional responses involved the up-regulation of dendritic spine morphogenesis pathways, synaptic potentiation programs, and actin cytoskeleton reorganization—all consistent with an involvement in natural recovery.

Connectome features of thoracic relay neurons

Our results thus far implied that $SC^{Vsx2::Hoxa7::Zfhx3\rightarrow lumbar}$ neurons contribute to the production of walking after natural recovery. Therefore, we hypothesized that these neurons must possess connectome features compatible with the requirements to walk after paralysis.

Visualization of the projectome from neurons embedded in the midthoracic spinal cord revealed dense projections throughout the lumbar gray matter (fig. S5A). To identify neuronal subpopulations possessing this projectome combined with a transcriptional phenotype consistent with our prioritized neuronal subpopulations (Fig. 1G), we compared the distribution and connectome of $Vsx2^{ON}$ neurons using intersectional genetics and viral tracing in $Vsx2^{Cre}$ mice. We found that $Vsx2^{ON}$ neurons accounted for 5.9% of neurons in the midthoracic spinal cord (fig. S5B), which agreed with the distribution of neurons identified in our snRNA-seq data (fig. S2, D and E). Tracing of midthoracic $Vsx2^{ON}$ neurons revealed the expected presence of dense projections throughout the lumbar spinal cord (fig. S5C).

We next asked whether midthoracic $Vsx2^{ON}$ neurons could be stratified into subpopulations projecting locally versus over long distances. In the spinal cord, neurons with local versus long-distance projections can be differentiated by the expression of Zfhx3 (*15*) (fig. S2, C and D). To label long-distance projecting $Vsx2^{ON}$ neurons, we infused rAAV2-Ef1α-DIO-Flpo into the lumbar spinal cord of $Vsx2^{Cre}$ mice followed by injections of AAV5-Con/Fon-eYFP (enhanced yellow fluorescent protein) into the midthoracic spinal cord (Fig. 2A, fig. S5D, and movie S1). This strategy enabled the exclusive labeling of $Vsx2^{ON}$ neurons that projected to the lumbar spinal cord (Fig. 2A, fig. S5D, and movie S1). We found that Zfhx3 and Vsx2 colocalized only in neurons projecting to this region ($SC^{Vsx2::Hoxa7::Zfhx3\rightarrow lumbar}$) (Fig. 2B) (*15*). Quantification of local ($Vsx2^{ON}Zfhx3^{OFF}$) versus long-distance projecting ($Vsx2^{ON}Zfhx3^{ON}$) $Vsx2^{ON}$ neurons revealed a near-equal distribution of these two subpopulations throughout the midthoracic spinal cord (fig. S5, D and E). These findings confirmed that a subset of $Vsx2^{ON}$ neurons embedded in the midthoracic spinal cord coexpress Zfhx3 and project to the lumbar spinal cord.

We reasoned that to function as relays of supraspinal commands, $SC^{Vsx2::Hoxa7::Zfhx3\rightarrow lumbar}$ neurons must also receive direct projections from key supraspinal neurons involved in the recovery of walking after paralysis. To expose this connectome, we infused AAV5-CMV-TurboRFP (CMV, cytomegalovirus; RFP, red fluorescent protein) into the ventral gigantocellular nucleus (vGi), because vGi neurons are essential for this recovery (*37*), followed by infusions of rAAV2-hSyn-GFP into the lumbar spinal cord and labeling of Vsx2 and vGlut2 synaptic puncta (Fig. 2C). As anticipated, we found that $SC^{Vsx2::Hoxa7::Zfhx3\rightarrow lumbar}$ neurons located in the midthoracic spinal cord receive projections from the vGi (Fig. 2C), and that this projection pattern is maintained after natural recovery (fig. S5, F and G).

These results indicated that among the diverse populations of neurons in the midthoracic spinal cord (*15*, *31*, *35*, *38*–*40*), $SC^{Vsx2::Hoxa7::Zfhx3\rightarrow lumbar}$ neurons were not only the most transcriptionally perturbed neuronal subpopulation during natural recovery but also exhibited the relevant anatomical profile to relay supraspinal commands past the incomplete SCI to the lumbar spinal cord.

Regeneration of axons to their natural target region after complete SCI

We previously found that providing factors essential for axon growth during development supported axon regeneration across anatomically complete SCIs into viable neural tissue located one segment below the injury, but that this regrowth did not restore walking (*1*). On the basis of our findings above, we hypothesized that recovery of walking after complete SCI could be achieved by reestablishing the natural projection patterns of neuronal subpopulations that contribute to recovery of walking after incomplete SCI. We therefore sought to determine whether $SC^{Vsx2::Hoxa7::Zfhx3\rightarrow lumbar}$ neurons could be regenerated to reach their natural target region in the lumbar spinal cord.

To test this possibility, we adapted our previously established regeneration strategy that harnesses three developmental mechanisms (movie S2) (*1*). First, we reactivated the intrinsic growth capacity of neurons located above the SCI with viral overexpression of osteopontin (*Spp1*), insulin-like growth factor 1 (*Igf1*), and ciliary-derived neurotrophic factor (*Cntf*) (AAV-OIC) (*41*). Second, we induced the formation of axon growth–supportive substrates within the lesion with temporally delayed delivery of fibroblast growth factor 2 (FGF2) and epidermal growth factor (EGF). Third, we delivered biomaterial depots of glial-derived neurotrophic factor (GDNF) as a chemoattractive agent below the injury (*1*, *42*, *43*). Analysis of snRNA-seq data confirmed the expression of GDNF receptor, *Gfra1*, and *Ret* in $SC^{Vsx2::Hoxa7::Zfhx3\rightarrow lumbar}$ neurons, both of which are required for appropriate GDNF signaling, and immunohistochemistry of $Vsx2^{ON}$ axons traced with AAV5-Con/Fon-eYFP validated expression of the GDNF receptor within the soma and along the axons of $SC^{Vsx2::Hoxa7::Zfhx3\rightarrow lumbar}$ neurons (Fig. 2B).

Consistent with our previous observations (*1*), we found that stimulated, supported, and

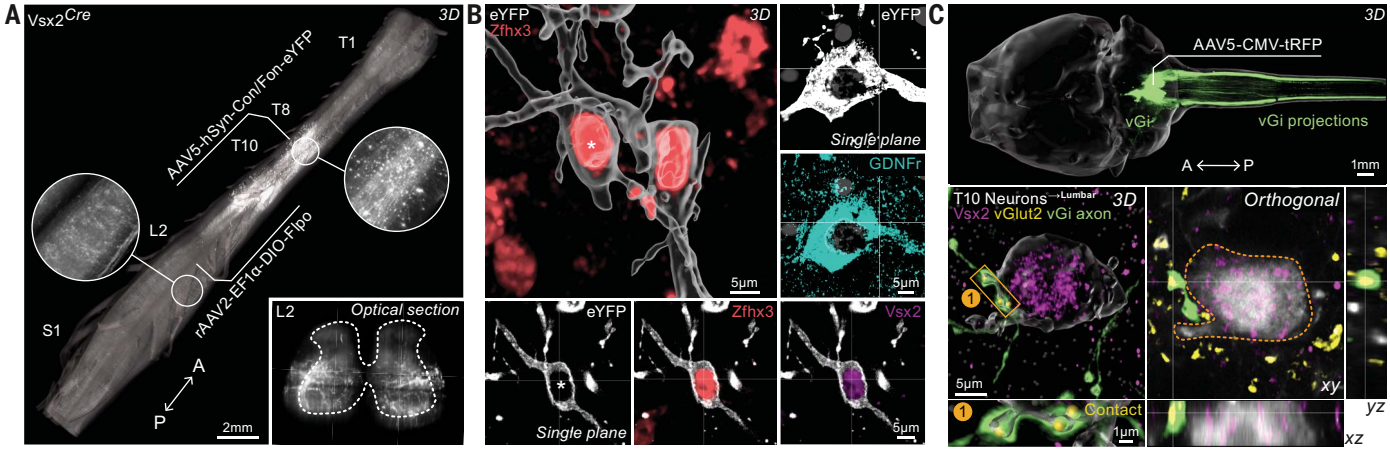

Fig. 2. Projection and connectome features of $SC^{Vsx2::Hoxa7::Zfhx3\rightarrow lumbar}$ neurons. (**A**) Whole spinal cord visualization of projections from Vsx2 neurons in the lower thoracic spinal cord that project to walking execution centers. Insets illustrate the starter neurons labeled using intersectional viral tracing, and their projections in the lumbar spinal cord. (**B**) Vsx2 neurons with projections to walking execution centers express Zfhx3, a key marker of projection neuronal subpopulations. These neurons also express Gdnfr on the neuron soma as well as along the axon. (**C**) Overview of the experimental approach enabling anterograde viral tracing of ventral gigantocellular nuclei (vGi) neurons in both uninjured mice and mice that underwent natural repair. A 3D view of synapse-like contact of Vsx2 neurons in the lower thoracic spinal cord with vGi virally traced projections, indicated with the presynaptic marker, vGlut2.

chemoattracted axons regrew through astrocyte borders, across the fibrotic scar, and into viable neural tissue below a complete SCI (fig. S6A). Nevertheless, regenerating axons terminated only one segment below the injury where the most distal GDNF-containing biomaterial depot had been infused. Accordingly, behavioral assessments conducted at 4 weeks after injury failed to detect any recovery (fig. S6B). This observation contrasted with the natural recovery of walking observed by 4 weeks after incomplete SCI, involving $SC^{Vsx2::Hoxa7::Zfhx3\rightarrow lumbar}$ neurons whose axons terminated within the lumbar spinal cord located several segments more distally (Figs. 1F and 2A).

We therefore reasoned that the recovery of walking after complete SCI cannot be achieved simply by bridging the lesion gap with short-distance or undirected regeneration, but that one of the key additional requirements must be to propel axons to their natural target region in the lumbar spinal cord. To achieve such long-distance and directed regeneration, we placed an additional depot of chemoattractive GDNF into the lumbar spinal cord (fig. S6C). However, this additional depot attracted comparatively few axons to the targeted lumbar region (figs. S6C and S7B), and behavioral assessments again failed to detect any recovery (fig. S6D).

We then posited that the relatively slow time course of long-distance axon growth, maturation, and synapse formation might require a more sustained and higher concentration of chemoattractive growth factor delivery than was provided by the biomaterial depot (*44*). To test this possibility, we engineered a lentivirus to provide sustained delivery of growth factor (*45*). Replacing biomaterial depots with lentivirus-mediated GDNF expression enabled an extensive regrowth of axons to their natural target region over two segments distally (Fig. 3, A to C; fig. S7; and movie S2), further demonstrating that appropriate chemoattraction gradients can guide directed long-distance axon regeneration in a manner similar to that of development (*46*).

To determine whether regenerated axons included those originating from $SC^{Vsx2::Hoxa7::Zfhx3\rightarrow lumbar}$ neurons, we infused rAAV2-hSyn-KASH-eGFP into the lumbar spinal cord. This strategy exclusively expressed eGFP in neurons whose axons had regrown sufficient distances to reach the lumbar spinal cord (fig. S8A). Nuclei of $eGFP^{ON}$ neurons located above the injury were sorted for snRNA-seq, and the resulting transcriptional profiles were integrated into our atlas of the thoracic spinal cord (fig. S8, B to G). Comparing the distribution of $eGFP^{ON}$ neurons to the distribution of neuronal subpopulations in the uninjured spinal cord showed that $SC^{Vsx2::Hoxa7::Zfhx3\rightarrow lumbar}$ neurons were the main virally labeled subpopulation, confirming the successful regeneration of this neuronal subpopulation to its natural target region (*47*) (Fig. 3E and fig. S8, H and I). Retrograde tracing coupled with immunohistochemistry of Vsx2 confirmed these results (Fig. 3F and fig. S8J). Transcriptional profiles showed that, compared to all other neuronal subpopulations, regenerated $SC^{Vsx2::Hoxa7::Zfhx3\rightarrow lumbar}$ neurons up-regulated axon regeneration pathways, Igf receptor signaling, and synaptic formation and transmission programs, as well as axon extension and maturation pathways, consistent with their regeneration and stabilization within the lumbar spinal cord (fig. S8K).

To test whether regenerated $SC^{Vsx2::Hoxa7::Zfhx3\rightarrow lumbar}$ neurons projected to the lumbar spinal cord in a manner similar to that found in uninjured mice, we injected AAV5-hSyn-flex-tdTomato into the thoracic spinal cord of $Vsx2^{Cre}$ mice that had undergone regeneration after complete SCI. We combined this tract tracing with immunolabeling of $Vsx2^{ON}$ and $Chat^{ON}$ neurons in the lumbar spinal cord. Regenerated axons were found around, and made contacts with, these neuronal subpopulations that are known to contribute to the production of walking (*18*, *22*, *23*, *31*–*34*) and are essential to regain walking after paralysis (*25*) (fig. S7E). Uninjured mice exhibited a similar projection pattern, suggesting that regenerated $SC^{Vsx2::Hoxa7::Zfhx3\rightarrow lumbar}$ neurons may inherently reform appropriate connections with their natural targets (fig. S7E) (*47*).

We also asked whether supraspinal commands could be detected below the anatomically complete SCI after regenerating $SC^{Vsx2::Hoxa7::Zfhx3\rightarrow lumbar}$ neurons to reach the lumbar spinal cord. We found that microstimulation of the vGi induced large motor evoked potentials in leg muscles, revealing that supraspinal centers had regained functional access to the lumbar spinal cord (Fig. 3D).

These results demonstrate that $SC^{Vsx2::Hoxa7::Zfhx3\rightarrow lumbar}$ neurons can be engineered to regrow functional axons to their natural target region in the lumbar spinal cord.

Substantial recovery of walking after anatomically complete SCI

Because our regenerative strategy chemoattracted and guided a molecularly defined neuronal subpopulation involved in natural recovery to regrow to their appropriate target region in the lumbar spinal cord, we anticipated that this strategy may restore walking after complete paralysis. We therefore performed longitudinal quantification of whole-body kinematics during walking in five separate cohorts of mice that underwent anatomically complete SCI and received the regeneration strategy. Evaluations showed that the SCI abolished leg movements in every mouse, such that even at 4 weeks after SCI, no mice exhibited any sign of recovery (fig. S9A). In all mice, the regenerative strategy promoted the growth of projections from $SC^{Vsx2::Hoxa7::Zfhx3\rightarrow lumbar}$ neurons to their natural target region in the lumbar spinal cord. This regrowth coincided with a progressive recovery of leg movements that emerged ~3 to 4 weeks after SCI (fig. S9, B to E). Final evaluations were performed at 8 weeks. In cohort one, five out of six mice displayed gait patterns that resembled those quantified in mice after incomplete SCI (Fig. 4, A to D; fig. S9F; and movie S2). These experiments were repeated in four subsequent cohorts, with a further 22 out of 24 mice (or a total of 27 out of 30 mice) demonstrating similar results (fig. S10, A to C). These results demonstrate that our regeneration strategy led to substantial recovery of walking after complete SCI. Notably, the mice that underwent regeneration did not walk as well as uninjured mice but instead exhibited a behavioral phenotype that was comparable to that of mice after incomplete SCI (*9*).

Our regenerative strategy promoted the regrowth of projections from neuronal subpopulations of the thoracic spinal cord other than $SC^{Vsx2::Hoxa7::Zfhx3\rightarrow lumbar}$ neurons (fig. S8H), and we thus could not exclude the involvement of these relatively less abundant neuronal subpopulations in the recovery of walking. Therefore, we tested the necessity of $SC^{Vsx2::Hoxa7::Zfhx3\rightarrow lumbar}$ neurons with regenerating projections to their appropriate target region in the lumbar spinal cord for the recovery of walking after regeneration, given their noted involvement in natural recovery after incomplete SCI. To do so, we first ablated these neurons in a third cohort of mice by expressing the diphtheria toxin receptor (DTR) in the thoracic spinal cord of $Vsx2^{Cre}$ mice (Fig. 4E; fig. S11, A and B; and movie S3). Eight weeks after SCI, all mice in cohort three that received our regeneration strategy had regained the ability to walk with gait patterns resembling those quantified in mice that had recovered walking after incomplete SCI (Fig. 4, F to H, and fig. S11, C to F). Administration of diphtheria toxin reparalyzed every tested mouse (Fig. 4, F to H; fig. S11, C to F; and movie S3). Anatomical analyses confirmed the near-complete ablation of $Vsx2^{ON}$ neurons in the thoracic spinal cord (fig. S11B). These results established the role of thoracic $Vsx2^{ON}$ neurons in the recovery of walking after regeneration. However, they did not establish the respective role of local versus projection $Vsx2^{ON}$ neurons.

Therefore, we tested the necessity of projections from $SC^{Vsx2::Hoxa7::Zfhx3\rightarrow lumbar}$ neurons to the lumbar spinal cord in the recovery of walking after complete SCI. We designed an intersectional chemogenetic strategy that allowed us to silence regenerated $SC^{Vsx2::Hoxa7::Zfhx3\rightarrow lumbar}$ neurons once mice demonstrated substantial recovery of walking. We infused rAAV2-Ef1α-DIO-Flpo into the lumbar spinal cord of a fourth cohort, followed by injections of AAV5-Con/Fon-hM4Di-mCherry into the thoracic spinal

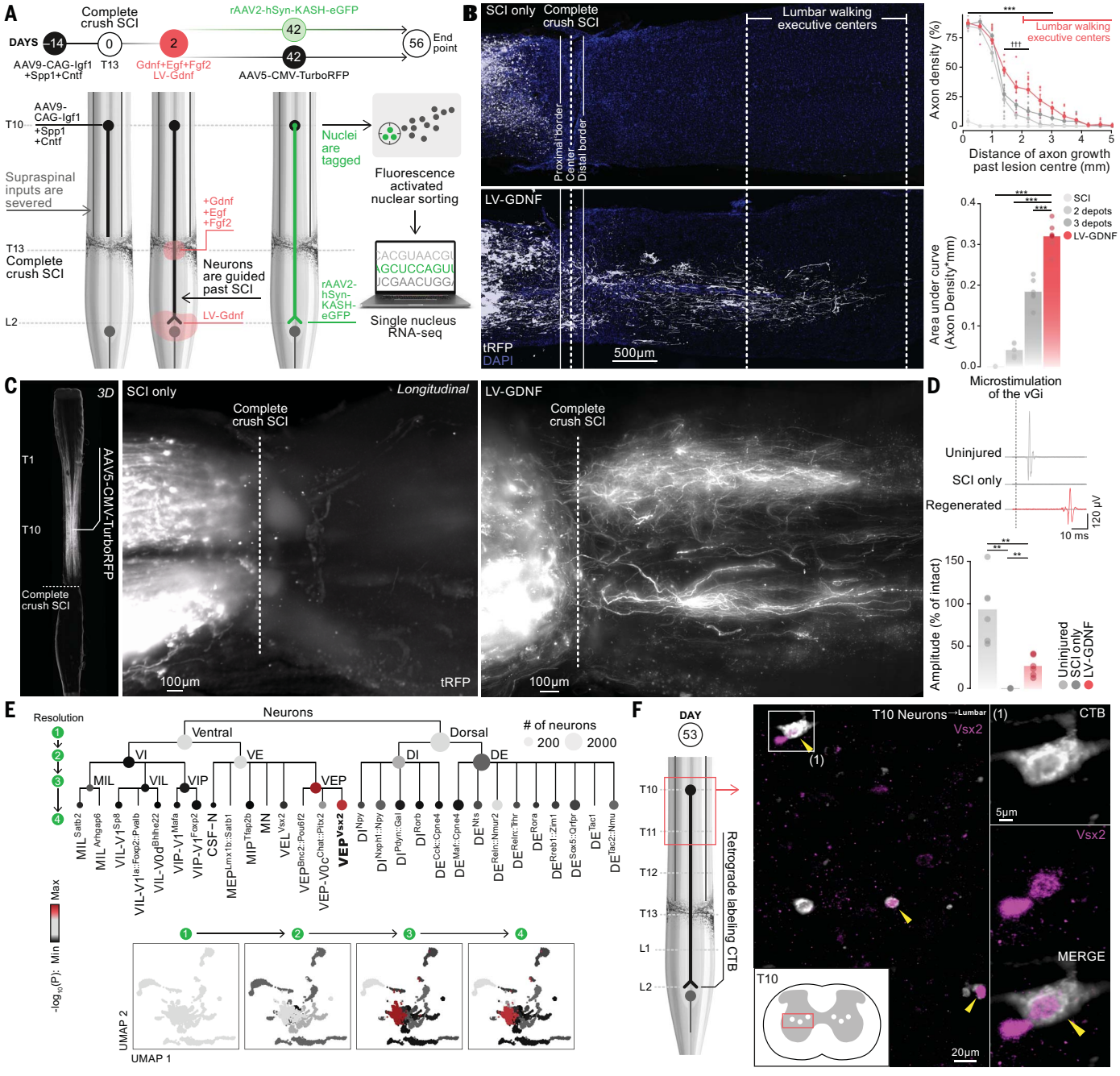

Fig. 3. SC$^{Vsx2::Hoxa7::Zfhx3\rightarrow lumbar}$ neurons regenerate across an anatomically complete SCI. (**A**) Overview of the experimental approach enabling regeneration across an anatomically complete SCI and into walking execution centers. (**B**) tRFP-labeled axons in composite tiled scans of horizontal sections from representative mice. Dotted lines demarcate astrocyte proximal and distal borders around the lesion core. Dashed line demarcates the lesion center. Line graph demonstrates axon density at specific distances past lesion centers (normalized to the density rostral to the lesion site). Statistics indicate Tukey honest significant difference (HSD) following one-way repeated measures analysis of variance (ANOVA). ***$P < 0.001$ LV-GDNF versus SCI only. †††$P < 0.001$ LV-GDNF versus 2 depots and 3 depots groups. (Right) Bar graph indicates the AUC of axon density in the walking execution center. Statistics indicate Tukey HSD following one-way ANOVA (all $P < 0.001$). (**C**) Whole spinal cord visualization of regenerating projections from the lower thoracic spinal cord that project to walking execution centers. (**D**) Representative individual electrophysiological traces after microstimulation of the ventral gigantocellular nucleus (vGi). (Bottom) Peak-to-peak amplitude of the evoked potentials in each experimental group, expressed as a percentage of uninjured mouse responses (Pairwise Wilcoxon rank-sum test, $P = 0.0064$). (**E**) (Top) The enrichment of regenerated neurons among neuronal populations of the mouse lumbar spinal cord is shown within a clustering tree of spinal cord neurons defined in four different clustering resolutions, demonstrating the robustness of these findings to the resolution at which transcriptionally defined neuronal subtypes are defined. (Bottom) The same enrichments are visualized on a progression of UMAPs. (**F**) Cholera toxin subunit B (CTB)–labeled regenerated neurons with Vsx2 immunohistochemical colabeling above the anatomically complete SCI.

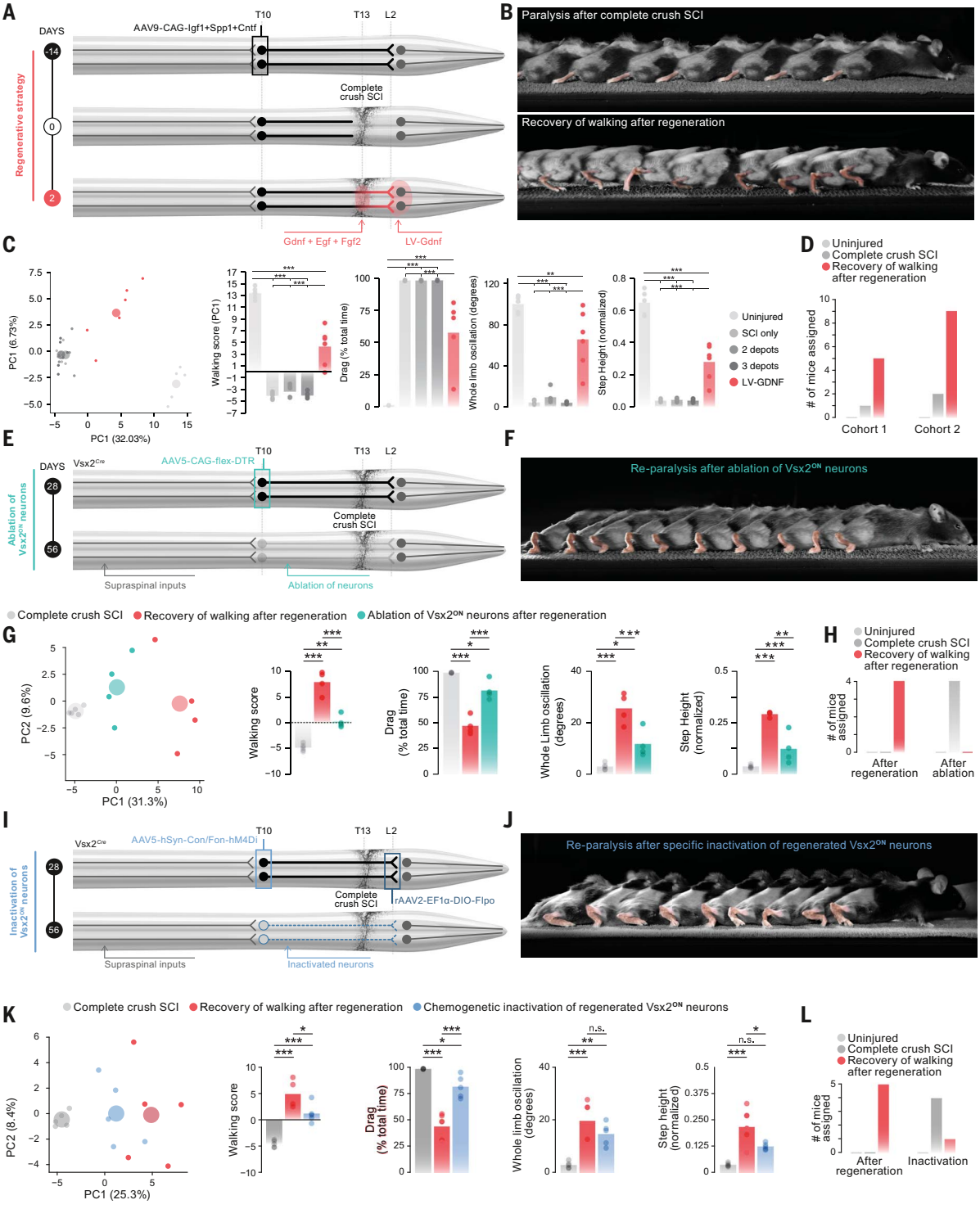

Fig. 4. Axons from SC$^{Vsx2::Hoxa7::Zfhx3 \rightarrow lumbar}$ neurons are necessary to restore walking after anatomically complete SCI. (**A**) Overview of the experimental approach enabling regeneration across an anatomically complete SCI and into walking execution centers. (**B**) Chronophotography of walking with (bottom) and without (top) mechanism-based combinatorial regeneration mimicking natural repair processes. (**C**) Walking was quantified using principal component analysis as described in Fig. 1F (n > 10 gait cycles per mouse, n = 6 mice per group, n = 5 mice in the uninjured and SCI only groups). Raw data and statistics are provided in data S6. (**D**) The number of mice from two cohorts of combinatorial treated animals at 8 weeks post-SCI that were assigned to each main experimental group. Mice were almost exclusively assigned by the classifier (see materials and methods, "Behavioral assessments") to the natural repair group, indicating that the walking patterns of regenerated mice most resemble those that underwent natural repair. (**E**) Experimental design for cell type–specific diphtheria toxin–mediated neuron ablation of Vsx2^{ON} neurons in the mid-thoracic spinal cord and intersectional chemogenetic inactivation of regenerated Vsx2^{ON} neurons following mechanism-based combinatorial regeneration. (**F**) Chronophotography of walking in Vsx2^{Cre} mice that received mechanism-based combinatorial regeneration mimicking natural repair processes coupled to viral injections of AAV5-CAG-FLEX-DTR to induce cell

type–specific neuronal ablation. (**G**) Walking was quantified using principal component analysis as described in Fig. 1F (n > 10 gait cycles per mouse, n = 4 mice per group, n = 5 mice in the SCI only group). Raw data and statistics are provided in data S8. (**H**) Mice were recorded before (left) and after (right) 1-week administration of diphtheria toxin. Bar graphs indicate the number of mice from each group that were assigned to each main experimental group (see materials and methods, "Behavioral assessments"). (**I**) As in (E) but for intersectional chemogenetic inactivation of regenerated $Vsx2^{ON}$ neurons in the mid-thoracic spinal cord. (**J**) As in (F) but for intersectional chemogenetic inactivation of regenerated $Vsx2^{ON}$ neurons in the mid-thoracic spinal cord. (**K**) As in (G) (n > 10 gait cycles per mouse, n = 5 mice per group). Raw data and statistics are provided in data S9. (**L**) As in (H) but for intersectional chemogenetic inactivation of regenerated $Vsx2^{ON}$ neurons in the mid-thoracic spinal cord.

cord (Fig. 4I; fig. S12, A and B; and movie S3). These mice all demonstrated the expected recovery of walking. The administration of clozapine-*N*-oxide (CNO) immediately impaired walking in all tested mice, leading to gait patterns that resembled those of mice that had not undergone regeneration (Fig. 4, J to L; fig. S12, B to D; and movie S3). By contrast, a fifth cohort of mice that did not receive AAV5-Con/Fon-hM4Di-mCherry infusions were unaffected by CNO administration (fig. S12E). These findings established that regenerated projections from $SC^{Vsx2::Hoxa7::Zfhx3 \rightarrow lumbar}$ neurons to their natural target region in the lumbar spinal cord contribute to the substantial recovery of walking after complete SCI.

Discussion

In this study, we investigated the degree to which recovery of function after anatomically complete SCI will require targeting characterized neurons and regenerating the axons from those neurons not simply across lesions but also to guide them to reach their natural target regions. To address this question, we first characterized the molecular identity of the neuronal subpopulations in the thoracic spinal cord that restore walking by relaying supraspinal commands past an incomplete SCI (*9*). We then traced the connectome of these neurons and found that their natural projection pattern extends several segments caudally to the lumbar spinal cord, where the neurons that produce walking reside. We then used our multipronged regeneration strategy (*1*) to stimulate the axons of these molecularly characterized neurons to regenerate through fibrotic lesion core tissue and into spared neural tissue caudal to the lesion. This strategy included reactivating dormant neuron-intrinsic growth programs, establishing matrix support for axons to grow through non-neural lesion core tissue, and supplying a gradient of chemoattraction to guide these axons to the caudal side of the injury (*1*). We show that regenerating these neurons to reach simply across lesions had no effect on the recovery of walking. By contrast, refining our strategy to enable graded chemoattraction and guidance of regenerating axons to their natural target region in the lumbar spinal cord promoted substantial recovery of walking after complete SCI. We applied projection-specific snRNA-seq to identify the neuronal subpopulations with regenerating axons past a complete SCI and demonstrated that our strategy regenerated axons from the neuronal subpopulations that restore walking after incomplete SCI.

Our causation-testing loss-of-function experiments show that the restoration of function was dependent on the regenerated axons of characterized neurons. To chemoattract regenerating axons, we expressed GDNF, a pleiotropic growth factor with the potential to affect different cells. Potential limitations of our study are that it is possible that GDNF may have had unexplored effects on lumbar spinal cord cells in such a way as to facilitate the reformation of functional connections, or that simply greater bulk regeneration may account for the better functional outcome.

These findings show that reestablishing the projections of molecularly defined neuronal subpopulations to their natural target region forms an essential yet previously unidentified requirement for axon regeneration strategies aimed at restoring lost neurological functions. This understanding has important implications for the design of therapies for larger mammals and humans, because the potentially long distance over which regenerated projections will have to grow to restore function may require strategies with complex spatial and temporal features.

We posit that applying the principles demonstrated here of (i) identifying and regenerating the axons of functionally relevant neuronal subpopulations, (ii) determining the requirements for reactivating neuron-specific developmental growth programs, (iii) identifying chemoattractants able to guide different types of transected axons past lesions to reach their natural target regions, and eventually combining these biological repair principles with complementary neuromodulation strategies (*10*, *14*, *48*), will unlock the framework to achieve meaningful repair of the injured spinal cord and may expedite repair after other forms of central nervous system injury and disease (*49*–*51*).

REFERENCES AND NOTES

1. M. A. Anderson *et al*., *Nature* **561**, 396–400 (2018).
2. F. Sun *et al*., *Nature* **480**, 372–375 (2011).
3. M. A. Anderson *et al*., *Nature* **532**, 195–200 (2016).
4. Z. He, Y. Jin, *Neuron* **90**, 437–451 (2016).
5. P. Lu *et al*., *Cell* **150**, 1264–1273 (2012).
6. G. H. D. Poplawski *et al*., *Nature* **581**, 77–82 (2020).
7. G. Kong *et al*., *Nat. Metab.* **2**, 918–933 (2020).
8. B. J. Hilton *et al*., *Neuron* **110**, 51–69.e7 (2022).
9. G. Courtine *et al*., *Nat. Med.* **14**, 69–74 (2008).
10. B. Chen *et al*., *Cell* **174**, 521–535.e13 (2018).
11. K. C. Murray *et al*., *Nat. Med.* **16**, 694–700 (2010).
12. M. V. Sofroniew, *Nature* **557**, 343–350 (2018).
13. L. Friedli *et al*., *Sci. Transl. Med.* **7**, 302ra134 (2015).
14. R. van den Brand *et al*., *Science* **336**, 1182–1185 (2012).
15. P. J. Osseward II *et al*., *Science* **372**, 385–393 (2021).
16. J. Ericson *et al*., *Cell* **90**, 169–180 (1997).
17. T. M. Jessell, *Nat. Rev. Genet.* **1**, 20–29 (2000).
18. J. Bouvier *et al*., *Cell* **163**, 1191–1203 (2015).
19. E. Azim, J. Jiang, B. Alstermark, T. M. Jessell, *Nature* **508**, 357–363 (2014).
20. C. Pivetta, M. S. Esposito, M. Sigrist, S. Arber, *Cell* **156**, 537–548 (2014).
21. L. Ruder, A. Takeoka, S. Arber, *Neuron* **92**, 1063–1078 (2016).
22. K. J. Dougherty, O. Kiehn, *J. Neurosci.* **30**, 24–37 (2010).
23. S. A. Crone *et al*., *Neuron* **60**, 70–83 (2008).
24. A. E. Stepien, M. Tripodi, S. Arber, *Neuron* **68**, 456–472 (2010).
25. C. Kathe *et al*., *Nature* **611**, 540–547 (2022).
26. W. A. Alaynick, T. M. Jessell, S. L. Pfaff, *Cell* **146**, 178–178.e1 (2011).
27. S. Arber, *Neuron* **74**, 975–989 (2012).
28. S. Grillner, T. M. Jessell, *Curr. Opin. Neurobiol.* **19**, 572–586 (2009).
29. O. Kiehn, *Nat. Rev. Neurosci.* **17**, 224–238 (2016).
30. K. J. Dougherty, O. Kiehn, *Ann. N. Y. Acad. Sci.* **1198**, 85–93 (2010).
31. M. Hayashi *et al*., *Neuron* **97**, 869–884.e5 (2018).
32. K. J. Dougherty *et al*., *Neuron* **80**, 920–933 (2013).
33. F. Bretzner, R. M. Brownstone, *J. Neurosci.* **33**, 14681–14692 (2013).
34. J. M. Cregg *et al*., *Nat. Neurosci.* **23**, 730–740 (2020).
35. M. A. Skinnider *et al*., *Nat. Biotechnol.* **39**, 30–34 (2021).
36. J. W. Squair, M. A. Skinnider, M. Gautier, L. J. Foster, G. Courtine, *Nat. Protoc.* **16**, 3836–3873 (2021).
37. L. Asboth *et al*., *Nat. Neurosci.* **21**, 576–588 (2018).
38. A. Zeisel *et al*., *Cell* **174**, 999–1014.e22 (2018).
39. J. W. Squair *et al*., *Nat. Commun.* **12**, 5692 (2021).
40. A. Sathyamurthy *et al*., *Cell Rep.* **22**, 2216–2225 (2018).
41. F. Bei *et al*., *Cell* **164**, 219–232 (2016).
42. L.-X. Deng *et al*., *J. Neurosci.* **33**, 5655–5667 (2013).
43. A. Blesch, M. H. Tuszynski, *J. Comp. Neurol.* **467**, 403–417 (2003).
44. B. Song *et al*., *Biomaterials* **33**, 9105–9116 (2012).
45. L. T. Alto *et al*., *Nat. Neurosci.* **12**, 1106–1113 (2009).
46. R. W. Sperry, *Proc. Natl. Acad. Sci. U.S.A.* **50**, 703–710 (1963).
47. J. N. Dulin *et al*., *Nat. Commun.* **9**, 84 (2018).
48. H. Lorach *et al*., *Nature* **618**, 126–133 (2023).
49. J. W. Squair, M. Gautier, M. V. Sofroniew, G. Courtine, M. A. Anderson, *Curr. Opin. Biotechnol.* **72**, 48–53 (2021).
50. M. A. Anderson, *Neurosurg. Clin. N. Am.* **32**, 397–405 (2021).
51. M. A. Anderson *et al*., *Nat. Neurosci.* **25**, 1584–1596 (2022).

ACKNOWLEDGMENTS

This work was supported by the Defitech Foundation, Wings for Life, Riders4Riders, Wyss Center for Bio and Neuroengineering, Swiss National Science Foundation (PZ00P3_185728 to M.A.A. and PZ00P3_208988 to J.W.S.); the Morton Cure Paralysis Foundation (to M.A.A.); the ALARME Foundation (to M.A.A. and G.C.); the Dr. Miriam and Sheldon G. Adelson Medical Foundation (to M.V.S., Z.H., and T.J.D.); Wings for Life (M.A.A., M.V.S., M.A.S., and M.M.); Friedrich Flick Förderungsstiftung through Wings for Life (M.A.A. and G.C.); Holcim-Stiftung Foundation (to J.W.S.); and the Canadian Institutes for Health Research (to J.W.S.). We are grateful to J. Ravier and M. Burri for the illustrations and to L. Batti and I. Gantar from the Advanced Lightsheet Imaging Center (ALICe) at the Wyss Center for Bio and Neuroengineering, Geneva, for their assistance with lightsheet imaging. **Funding:** This work was supported in part using the resources and services of the Gene Expression Core Facility, and the Bertarelli Platform for Gene Therapy at the School of Life Sciences of EPFL. **Author contributions:** J.W.S., J.B., M.V.S., G.C., and M.A.A. conceptualized and designed experiments; J.W.S., M.M., A.d.C., N.D.J., N.C., C.K., T.H., S.C., L.B., K.G., A.L., Q.B., and M.A.A. conducted experiments; J.W.S., M.M., M.G., A.d.C., M.A.S., N.D.J., A.L., A.L., V.A., Q.B., and M.A.A. analyzed the data. T.J.D., B.L.S., R.K., and Z.H. contributed essential resources. J.W.S., M.V.S., G.C., and M.A.A. prepared the manuscript. **Competing interests:** The authors declare no direct competing financial interests. G.C. is a consultant and minority shareholder of ONWARD medical, a

company with no relationships with the presented work. Z.H. is a consultant of Axonis, SpineX, and Myrobalan Therapeutics. J.W.S., M.A., B.L.S., and G.C. have filed a patent in relation with this work.
Data availability: Data that support the findings and software routines developed for the data analysis will be made available upon reasonable request to the corresponding authors. Source data are provided with this paper. Raw sequencing data and count matrices have been deposited to the Gene Expression Omnibus (GSE198949).
Code availability: Augur is available from GitHub (https://github.com/neurorestore/Augur).

SUPPLEMENTARY MATERIALS

science.org/doi/10.1126/science.adi6412
Materials and Methods
Figs. S1 to S12
References (*52*–*66*)
Movies S1 to S3
Data S1 to S9

Submitted 9 May 2023; resubmitted 5 July 2023
Accepted 18 August 2023
10.1126/science.adi6412

Recovery of walking after paralysis by regenerating characterized neurons to their natural target region

Jordan W. Squair, Marco Milano, Alexandra de Coucy, Matthieu Gautier, Michael A. Skinnider, Nicholas D. James, Newton Cho, Anna Lasne, Claudia Kathe, Thomas H. Hutson, Steven Ceto, Laetitia Baud, Katia Galan, Viviana Aureli, Achilleas Laskaratos, Quentin Barraud, Timothy J. Deming, Richie E. Kohman, Bernard L. Schneider, Zhigang He, Jocelyne Bloch, Michael V. Sofroniew, Gregoire Courtine, and Mark A. Anderson

Science, **381** (6664), .
DOI: 10.1126/science.adi6412

Editor's summary

Although several experimental approaches have shown positive results in axonal regeneration after spinal cord injury (SCI), complete recovery of motor functions remains an elusive target. Squair *et al*. hypothesized that restoration of complete axonal projection of a selected neuronal population to their natural target could promote better functional recovery. After using single-cell RNA sequencing to identify the most promising neuronal population, the authors showed that promoting axonal growth and path guidance to their natural target in this population restored walking in mice after complete SCI. By contrast, broad axonal restoration across the lesion had no effect, suggesting that a more targeted approach is necessary for functional recovery after SCI. —Mattia Maroso